Calibration of the BEMC calorimeter : STAR 2013 pp510 GeV

Devika Gunarathne*
Jinlong Zhang†

October 24, 2016

*Temple University
†Shandong University

Contents

List of Figures

List of Tables

Abstract

This note outlines the summary of procedure used to carry out the calibration of the Barrel Electromagnetic Calorimeter (BEMC) in the STAR Experiment at RHIC for the STAR run 2013 data set. Minimum Ionizing Particles (MIPs) provided the relative calibration for each of the 4800 BEMC towers, while electrons were used to find the absolute calibration separately for each of the 40 η-rings, which consist of 120 towers at each distinct η in the detector. Preliminary calibrations constant were obtained, along with systematic uncertainties calculated to be on the order of 3% for run 13 period 1 and 2% for run 13 period 2.

1 Introduction

The BEMC is a Pb-Scintillator sampling calorimeter that covers 2π in azimuth and from -1 to 1 in pseudo-rapidity, which is divided into 120 modules. Each module consists of 21 mega-tiles of scintillator and 20 layers of Pb. The mega-tiles are divided into 40 optically isolated sections covering approximately 0.05 $\times$ 0.05 in $\eta \times \phi$ space. The total depth is approximately $20X_0$ at η=0, which corresponds to the containment of electromagnetic showers up to $60GeV$. The tower high voltages were set so that a 60 GeV shower would be near the maximum of the 12 bit ADC readout. In 2013 RHIC ran in the proton-proton mode at $\sqrt{s} = 510GeV$. During the Run 13 data collection a new detector, the Heavy Flavor Tracker (HFT), was installed at STAR during day 126 to day 129 of the running period, which caused for a change in the geometrical properties of the detector. Therefore two sets of calibration gain constants were obtained by separately analyzing the data before (period 1, day 76 to day 126) and after (period 2, day 129 to day 161) the HFT insertion. The runs used for the calibration are the same as those used for the STAR 2013 WA_L analysis [1].

2 Relative gain calibration using MIPs

The method used in this calibration is the same as the one used in the STAR 2009 BEMC calibration [2] and STAR 2012 pp200 GeV BEMC calibration. First a relative tower by tower calibration is done using minimum ionizing particles (MIPs). This is done by identifying the characteristic ADC value in the MIP spectrum. The MIP energy deposition has a functional form as shown in Equation 1, which was determined via test beam data and simulation fits to spectra [2].

$$MIP = (264 \pm 4_{stat} \pm 13_{sys} MeV) \cdot \frac{1 + 0.056\eta^2}{\sin(\theta)} \tag{1}$$

where η is the pseudo-rapidity of the tower and θ is the scattering angle. From this relation one expects to see a peak approximately at 20 ADCs above pedestal, as shown in Figure 1.

To find the MIP peak, tracks with momentum, $p > 1$ GeV, which entered and exited the same tower were used. A single track per tower was considered in order to reduce the background energy deposition. A MIP ADC distribution was obtained per tower and it was fitted with a gaussian$\times$landau function which best described the signal and the background regions of the spectrum. The fitted mean vale was taken as the mean MIP ADC value for the given tower. For some towers a fit to the MIP distribution was not possible due to various reasons such as dead PMTs, hot towers, or other hardware failures. A quality analysis (QA) was done for every single tower to ensure the quality of the MIP peak extraction. Based on the results of the QA, towers with unacceptable MIP peak means, such as double peaks, significantly larger than expected MIP peaks, and towers with no MIP peaks were marked as towers having a "bad" status in the data base. The MIP means of remaining towers were marked with a "good" status and were then used to find the relative gain constants for each tower according to the formula in Equation 2.

$$C_{relative} = \frac{0.264(1 + 0.056 \cdot \eta^2)}{ADC_{mip} \cdot \sin(\theta)} \tag{2}$$

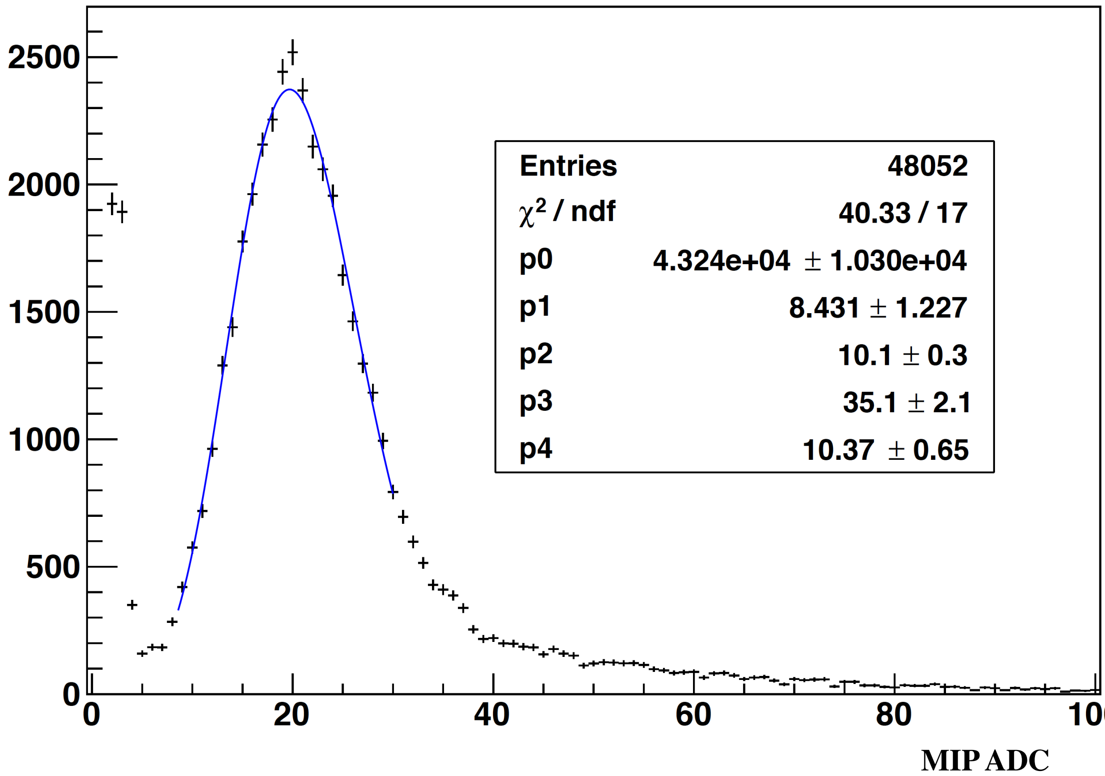

Figure 1: A typical MIP ADC distribution (black points) and gaussian×landau fit (in blue) for a single tower.

2.1 Time dependance of the MIP peak

The time dependance of the MIP peak was examined during the relative gain calibration. In order to do the evaluation, entire run 13 data set was divided in to 15 time periods, with each period containing approximately 6 days worth of consecutive runs. The average MIP peak value of each time period was then compared to the average MIP peak value of the subsequent time period. Figure 2 shows the difference between the average MIP peak value of each time period to the subsequent time period. Over the span of the Run 13 period 1 running, a change of approximately 2% in the MIP peak was observed. However during the Run13 period 2 running, the MIP peak was found to be fairly stable. Moreover, the mean MIP ADC values of the Run 13 p-p 510 GeV were compared to the corresponding Run 12 p-p 200 GeV and p-p 510 GeV calibrations. Changes to the MIP peak values during these running periods can be seen in Figure 3. As one would expect, the mean MIP peak value decreases from Run 12 to Run 13. According to the distributions, there is about a 3% difference found between the average MIP peak values of Run 12 p-p 200 and 510 GeV running, while only about a 1% difference is seen between the Run 12 and Run 13 p-p 510 GeV runnings.

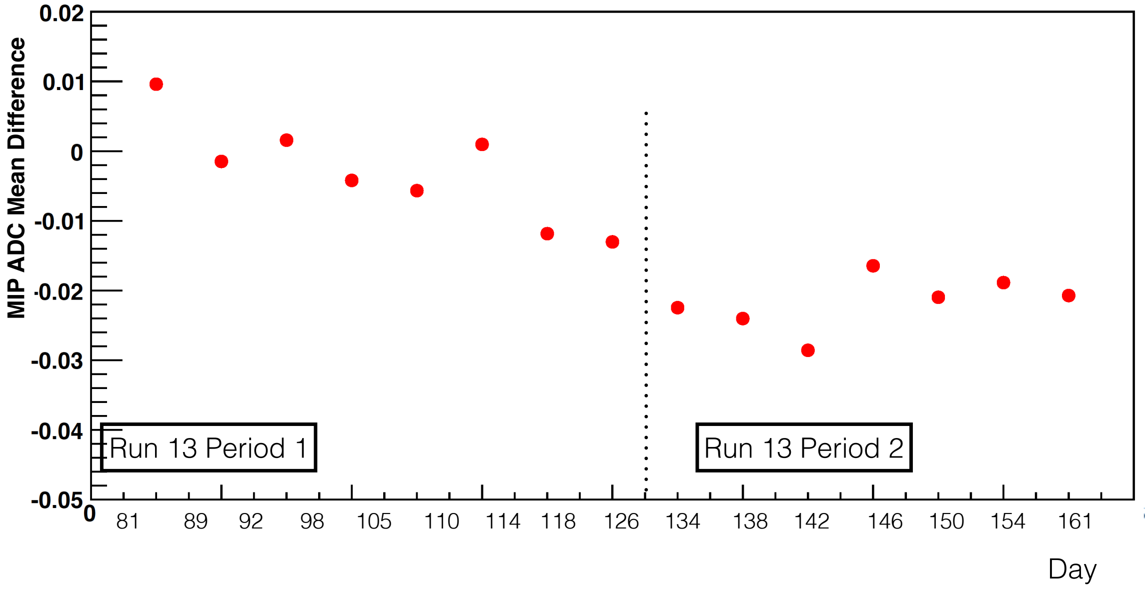

Figure 2: Time dependance of the MIP peak in run 13.

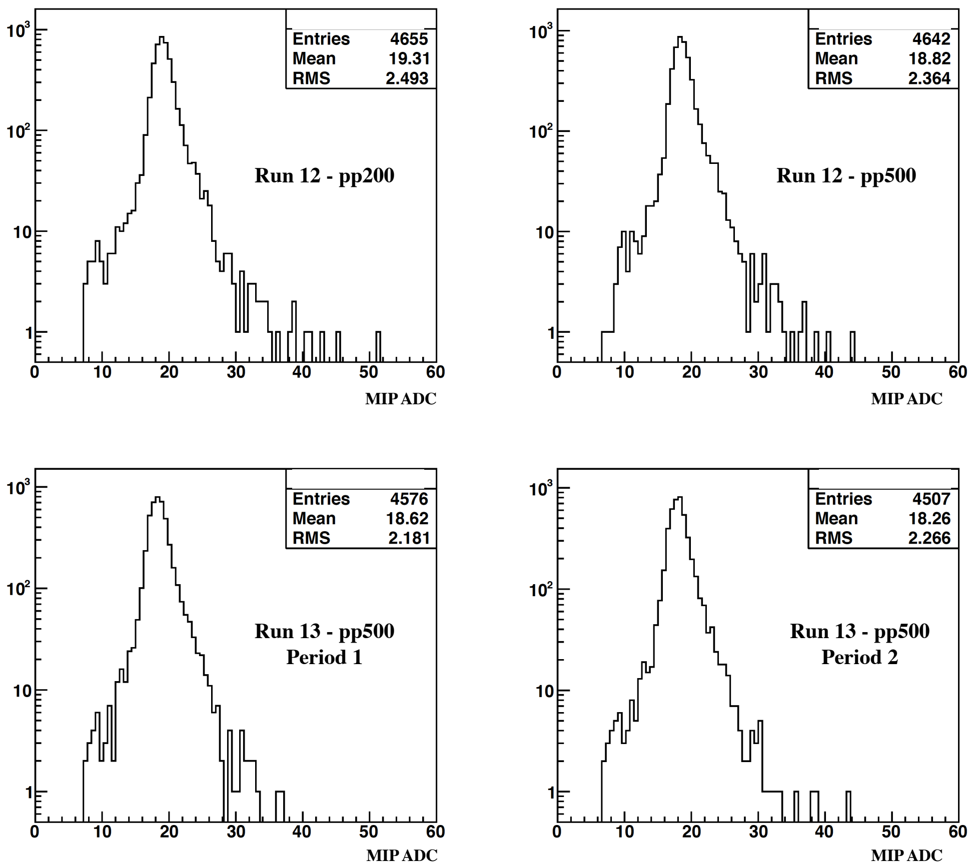

Figure 3: Distributions of the MIP peak values from STAR Run 12 p-p 200 GeV (upper left panel), Run 12 p-p 510 GeV (upper right panel), Run 13 510 GeV period 1 (bottom left), and Run 13 p-p 510 GeV period 2 (bottom right) running periods.

2.2 Summary

The relative gain constants of the calorimeter towers were obtained using MIPs. During the process 4.7% of the 4800 towers were identified as “bad” towers during Run

13 period 1 running, while 6.1% of towers were identified as “bad” in Run 13 period 2 running. The increase in “bad” towers for period 2 was found to be caused by a missing modulo in the calorimeter. Figure 4 shows $\eta - \phi$ distributions of relative gain constants of all the barrel towers from the Run 13 period 1 and 2 calibrations. The towers which were identified as being “good” towers were used to obtain an absolute gain constants by calibrating the electron’s energy to the tracking momentum through the energy over momentum ratio (E/p). Time dependance of the MIP peak values were also studied and found to vary by approximately 2% during the Run 13 period 1 running, and were fairly stable during the Run 13 period 2 running.

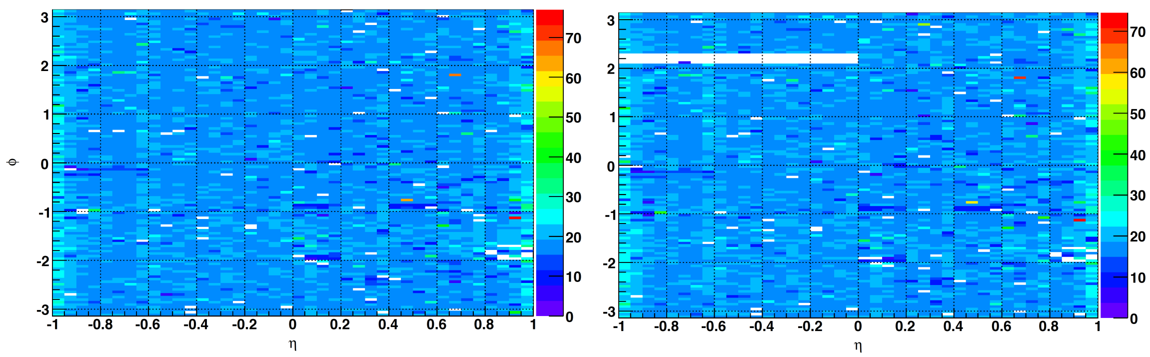

Figure 4: Relative gain constants of the calorimeter towers of Run 13 periods 1(left panel) and 2(right panel).

3 Absolute gain calibrations using Electrons

Absolute gain calibration constants were obtained by adjusting the relative gain constants using the electron shower energy spectra. Since electrons deposit all of their energy in the calorimeter towers, the strategy was to compare the deposited electron energy to the momentum of the electron track calculated from the TPC. For an ideal situation, assuming the electrons to be massless (a reasonable assumption for electron tracks with momentum on the order of GeV/c), the energy deposited in the calorimeter tower would be equal to the electron’s momentum, and thus $E/p = 1$. Unlike MIPs, abundant electrons are hard to find tower by tower. Therefore electrons that strike towers at a given pseudo-rapidity are added together (120 towers in each of 40 rings). Then the distribution of the electron’s E/p for a given ring was obtained considering all of the towers [120 towers] with in a ring. Conventionally, E is the energy deposition with in a single tower of the calorimeter where a electron track is matched from the TPC while p is the momentum of the track. The measured electron energy E from the calorimeter tower was corrected to take into effect of energy loss in material between the TPC and the BEMC and the pseudo-rapidity dependence by calculating correction factors in GEANT. These GENAT corrections factors were calculated for each pseudo rapidity ring as a function of $\Delta R = \sqrt{\Delta\phi^2 + \Delta\eta^2}$ from the center of the tower during the year 2009 [2] . The E/p obtained using this method refered to as the single tower method in this note.

In the Run 13 BEMC calibration, an alternative method (2×2 cluster method) was developed to obtain the tower energy E, by measuring the energy of the maximum

2×2 cluster inside a 3×3 cluster which also include the center tower where the electron track is matched. Figure 5 illustrates the single tower and the 2×2 cluster method. Once the E/p ratio is constructed for every candidate track, a average E/p value is then obtained by fitting the E/p distributions over all the tracks with in the 120 towers of each eta ring using a gaussian function for the signal and an exponential function to describe the background. A typical E/p distribution for electron tracks in a given eta ring ($\eta \sim 0.75$) is shown in Figure 6. The mean E/p value, was extracted from the gaussian mean of the fitted function and was then used to calculate the absolute calibration constant defined as,

$$C_{absolute} = \frac{C_{relative}}{\langle E/p \rangle} \tag{3}$$

where $C_{relative}$ is defined in Equation 1.

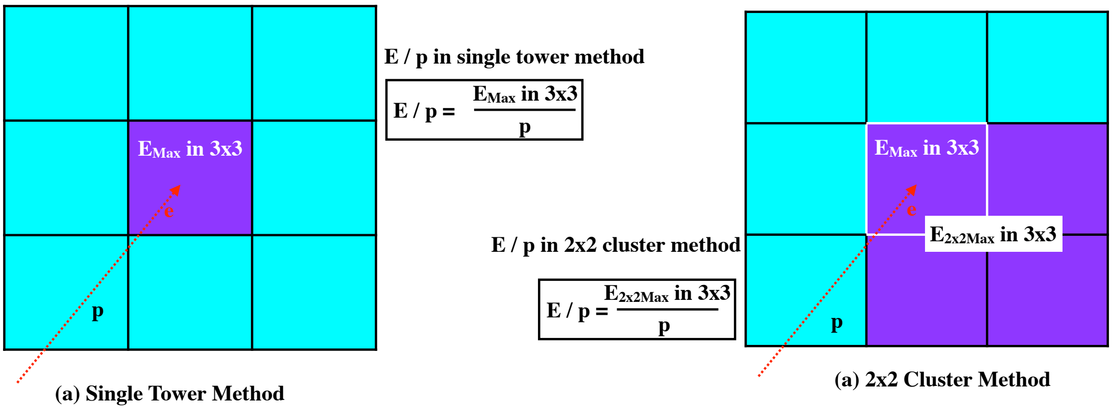

Figure 5: Methods used in the Run 13 BEMC absolute gain calibration.

3.1 Trigger option of the data sample

According to the BEMC calibration reports from previous years, the trigger biases in the data samples have contributed a significant amount of systematic uncertainty. Moreover, various momentum dependance of the electron E/p have been observed for different types of triggered events. Therefore in the Run 13 calibration, a study was conducted to find an unbiased electron sample. The high tower (HT) and non high tower (non HT) triggered events were used in the study. The HT trigger condition requires the tower energy to pass a set trigger threshold. Table 1 shows the various trigger conditions and tower energy threshold values for the trigger options used for this study.

Based on the previous studies, while the HT events have shown a clear momentum dependance, the non HT events have shown a stable E/p over a large range of the momentum. Similar performances were found for the HT trigger events (BHT1 and BHT3) and the non HT trigger events (JP2) of the Run 13 data set. Similar to the prior year's observations a clear momentum dependance was observed for the HT events (Figure 7a and 7b) and a stable behavior for non HT events (Figure 7c). The mean values of E/p from the fitted curve of the E/p distribution of the electrons in momentum slices of width 0.5 GeV is shown in Figure 7d. Near the thresholds,

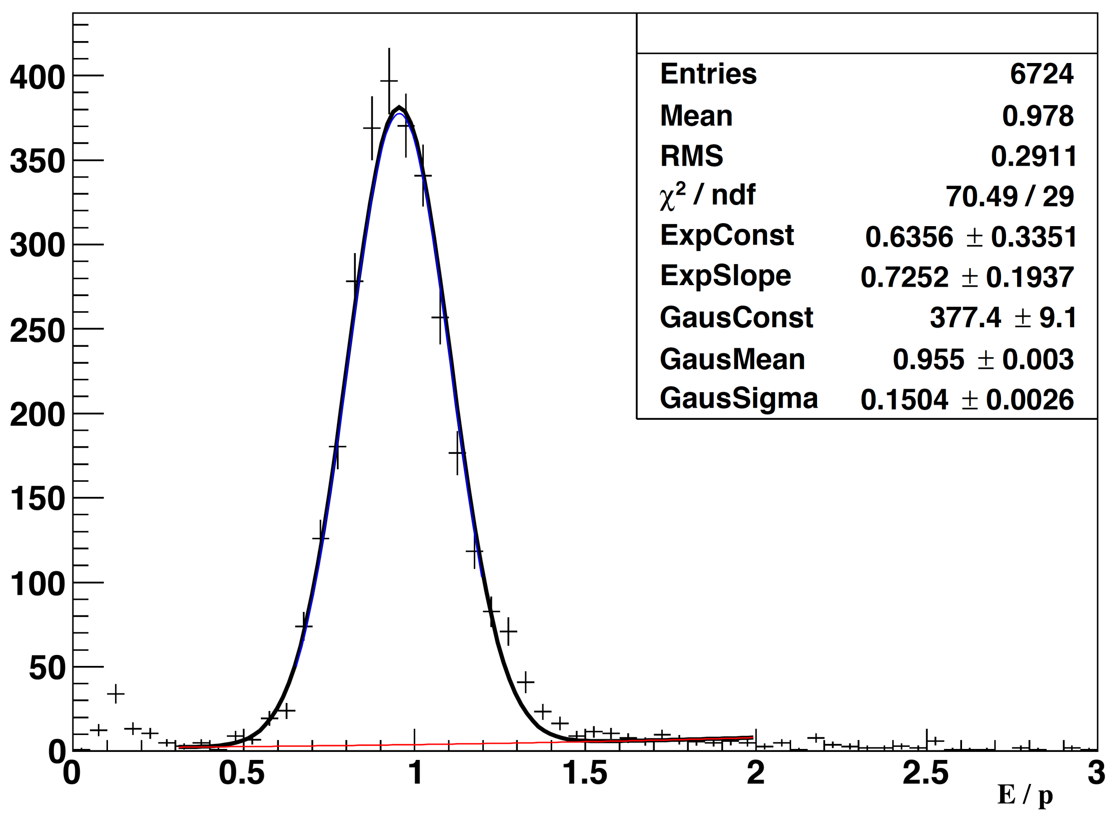

Figure 6: A typical electron E/p spectrum for one of the eta rings (black points), gaussian fit to the signal region (blue curve), exponential fit to the background region (red curve), and the sum of the two fits (black curve).

Trigger Name	**Trigger Thresh-old (GeV)**
Barrel High Tower Trigger 1 [BHT1→ didFire()]	4.25
Barrel High Tower Trigger 3 [BHT1→ didFire()]	7.75
Jet Patch Trigger 2 [JP2→ didFire()]	$\sim$ 14

Table 1: Trigger options used to select various data samples.

the HT events select electrons with a high E/p in comparison to those away from the threshold. In addition, a continuous drop in E/p with increasing momentum was seen well above the trigger threshold for the high tower events. More details about HT trigger momentum dependance can be seen in appendix A. This effect is clearly visible in the BHT1 events. Due to this strong momentum dependance of E/p, the BHT1 events were not used in this analysis. The JP2 and BHT3 events were used in this analysis in the momentum ranges of 0 to 10 GeV and 0 to 3 GeV respectively. The upper momentum limit for BHT3 was determined from the E/p distributions of momentum slices of width 0.5 GeV as shown in (Figure 8) in order to avoid possible trigger thresholds effects. For the BHT3 events a second background peak emerged at momentum values above 3 GeV. Therefore only events below a momentum of 3 GeV were used. In addition, the HT events showed a systematically lower E/p when compared to the JP2 events. This difference was added to the systematic uncertainty.

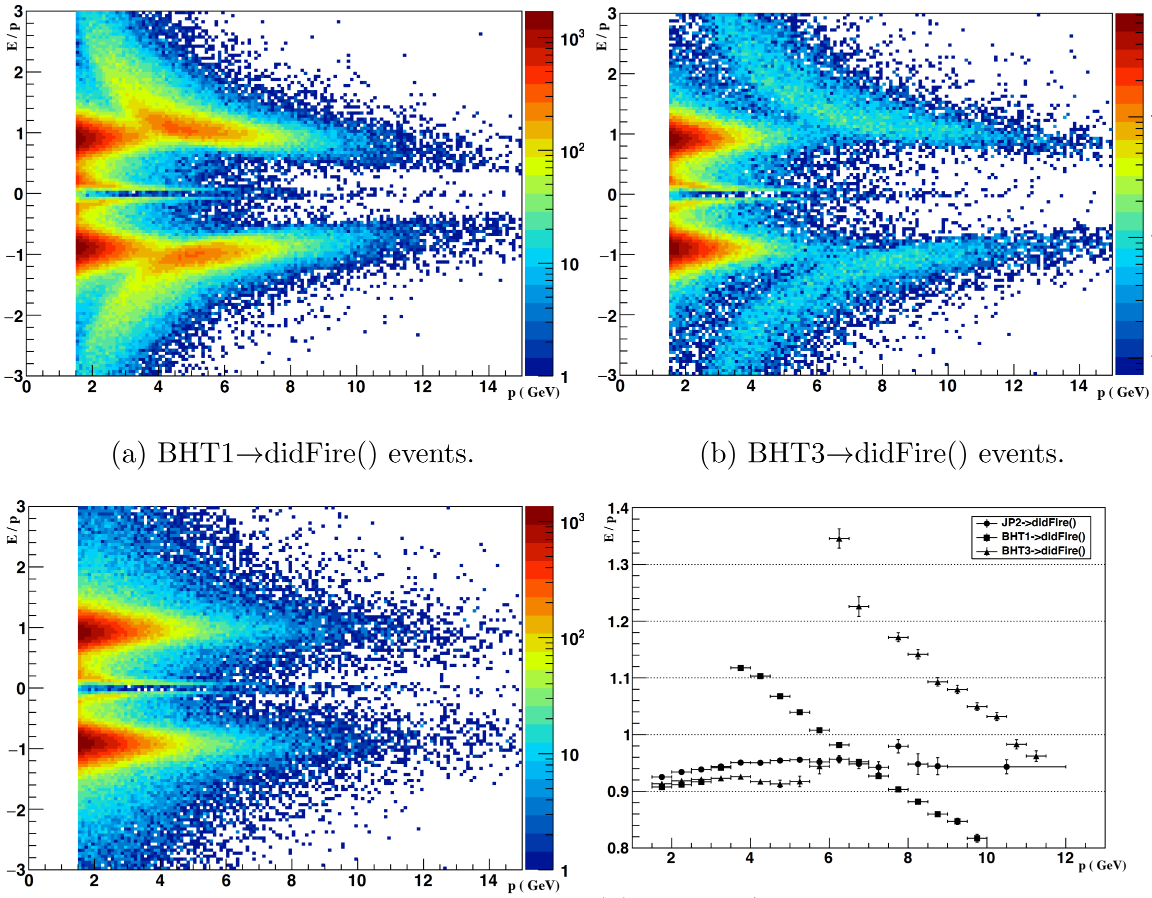

(a) BHT1→didFire() events.

(b) BHT3→didFire() events.

(c) JP2→didFire() events.

(d) Mean E/p of 0.5 GeV wide momentum slices.

Figure 7

3.2 Electron Selection Criteria

A set of vertex, track selection particle identification (PID), and calorimeter tower energy isolation cuts were used to select good electron candidates. Due to large amounts of pileup in the TPC, tracks with nHits > 25 were used. Primary vertices with a rank above 1e6 and $|Z_{vertex}| < 60cm$ were used. Candidate tracks were also required to have a dE/dX between 3.5e-6 and 5.0e-6 (Figure 10a). Furthermore for good electron PID, nSigmaElectron is required to be in between -1.0 and 2.0 (Figure 10b), while nSigmaPion is required to be above 3.0 (Figure 10c). In the single tower method, the energy is measured by matching the electron candidate tracks to a single tower and requiring that the track projection also exits the same tower and that no other tracks are matched to towers forming a 3×3 cluster around the track-matched tower (center tower). Furthermore, the center tower of the 3×3 cluster must also contain the maximum energy of the towers forming the cluster. These 3×3 cluster requirements help reduce the shower leakage from neighboring towers. The shower leakage

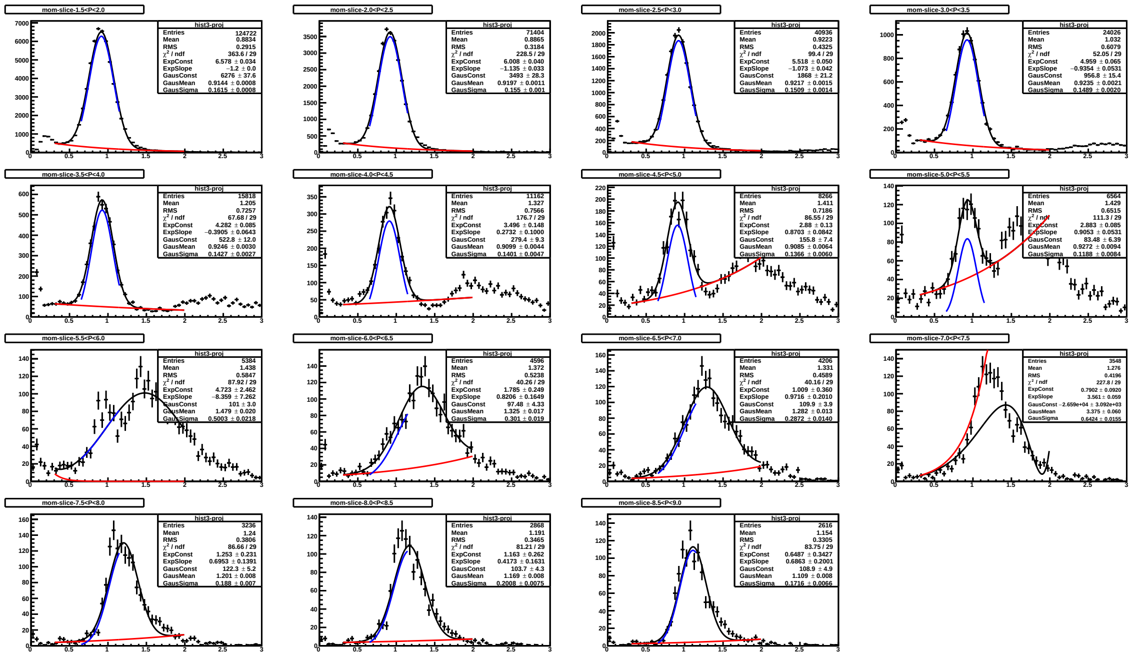

Figure 8: E/p distributions of momentum slices of width 0.5 GeV of BHT3 trigger events

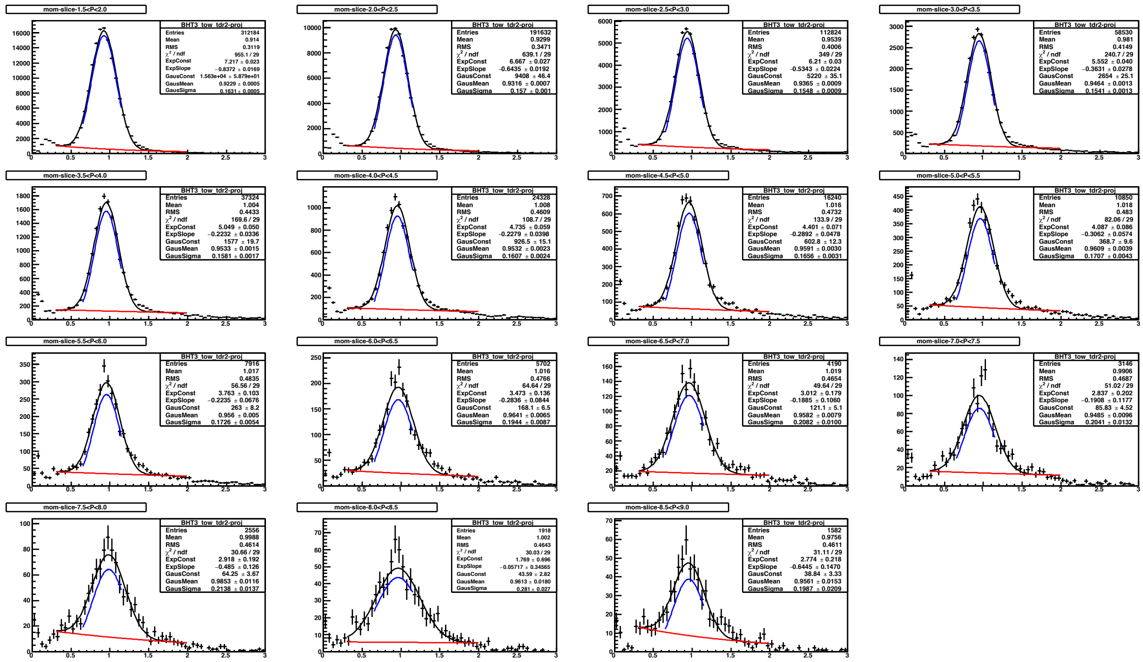

Figure 9: E/p distributions of momentum slices of width 0.5 GeV of JP2 trigger events

when using the single tower method is corrected using a GEANT based simulation, where correction factors are calculated based on the fiducial radius, which is defined as the distance between the center of the tower and where the track hits the tower face. Unfortunately, these corrections were found to be ineffective at fiducial radii above 0.02. Therefore a fiducial radius (TDR) cut of 0.02 was used. Finally, in this study electrons with in the momentum range of 2.0 GeV to 10 GeV were selected. A significant variation of E/p for low momentum (1.5 - 3 GeV) electrons was observed, and applied as part of the total systematic uncertainty in the tower gains.

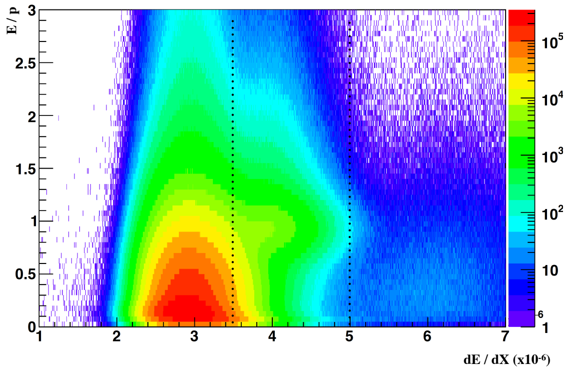

(a) Electron E/p as a function of dE/dX.

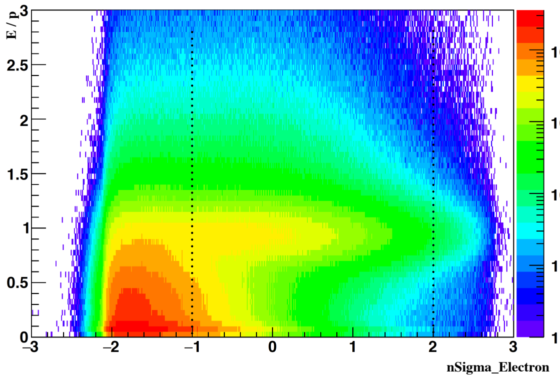

(b) Electron E/p as a function of nSigmaElectron.

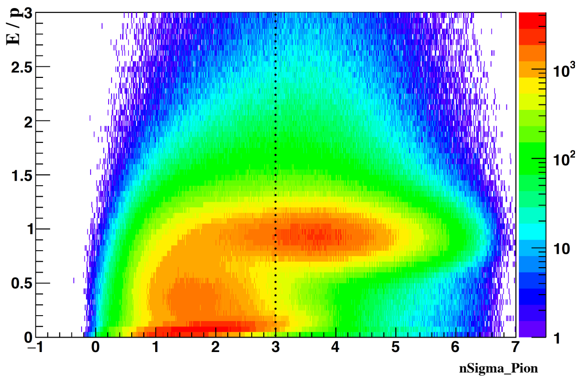

(c) Electron E/p as a function of nSigmaPion.

Figure 10

3.3 Electron's E/p values in pseudo-rapidity rings

The average E/p values were relatively constant at mid-rapidity, corresponding to the inner η rings (rings 3 to 38), and found to be within 5%. However at larger rapidities, corresponding to the outer η rings with $|\eta| \sim 1.0$ (rings 1,2,39, and 40), E/p was found to decreased by about 20%. The large variation at large rapidities was attributed to the increase in dead materials between the TPC and the front of the calorimeter tiles, which causes showers to begin earlier and allows more energy to escape the tower. In addition to this the systematically lower E/p behavior that was observed at low momentum (p ¡ 3.0 GeV) further decreased, which effectively enhanced this difference. As a result, the pow momentum cut of η rings 1, 2, 39 and 40 was increased from 2.0 to 3.0 GeV. Figure 11 shows the distribution of the average E/p values of all 40 η rings in the BEMC. Each ring covers a window of $\Delta\eta$ of 0.05. Rings 1 and 40 cover η ranges between [-1,-0.975] and [0.975,1] while rings 20 and 21 cover the η ranges between [-0.025,0] and [0,0.025], respectively. These E/p values were then used to calculate absolute gain values for each tower according to the formula shown in Equation 3.

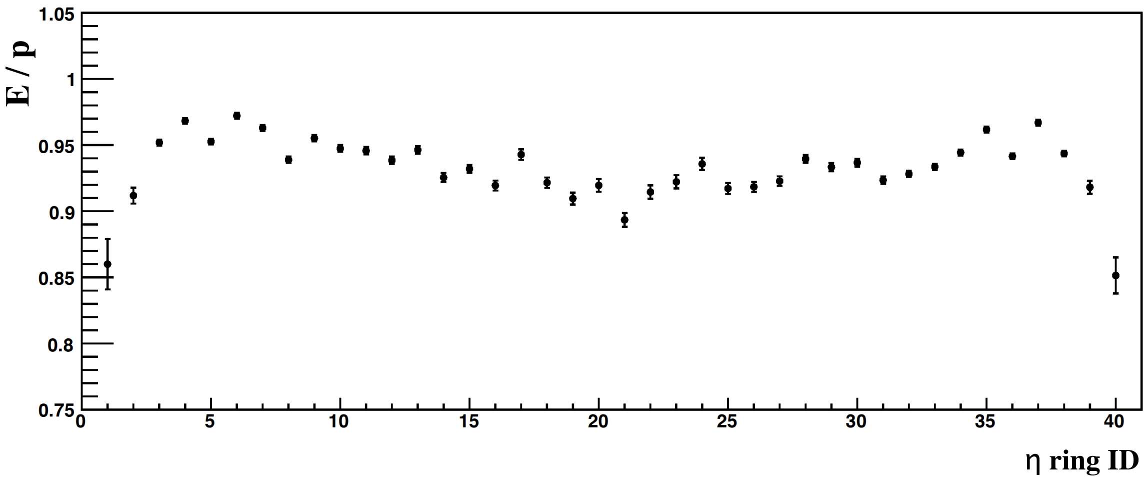

Figure 11: Mean electron E/P values for all 40 η rings in the BEMC.

4 Results

For the purpose of the preliminary W analysis, the absolute gain constants from the single tower method were used. A comparison of the average gain constants from previous year's BEMC calibration gain constants are shown in table 2. Table 2 shows the percentage difference of the average gain constants in each year/period compared to the Run 13 period 1 results. While Run 13 period 1 gains were approximately 3% larger than Run 9 p-p 200 GeV gains, they were approximately 5% larger than Run 12 p-p 200 GeV gains. Furthermore, the Run 13 period 2 gains were found to be 3% larger than the Run 13 period 1 gains. The consistency of the calorimeter gain constants, which were obtained at a low energy scale (0-15 GeV), were checked at a high energy scale using high energy probes such as the Z boson invariant mass and W boson Jacobean peak. This check revealed that the gain constants obtained at the low energy scale were consistent at high energy levels with in the systematic uncertainty as shown in Figures 12, 13 in comparison to MC.

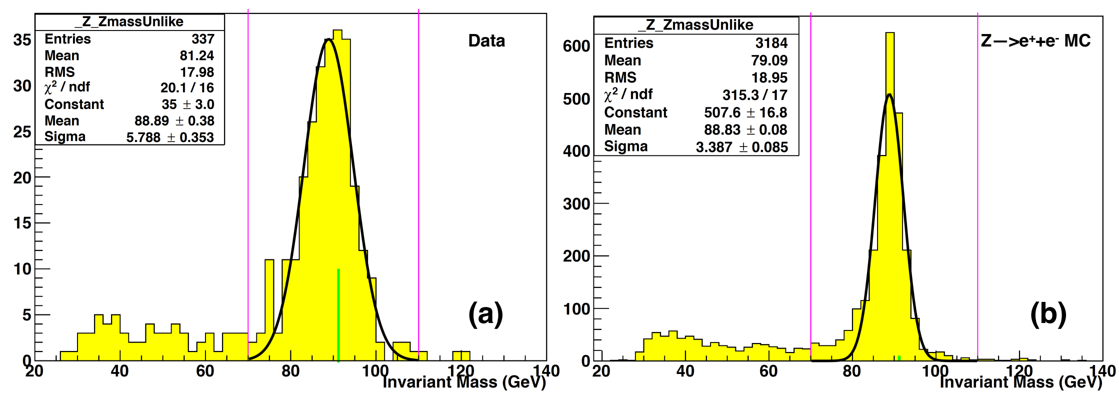

Figure 12: The invariant mass distribution of Z boson from STAR Run 2013 data (a) (after run 13 gains applied) and $Z \to e^+ + e^-$ MC (b) fitted with an gaussian function in the window [70,110].

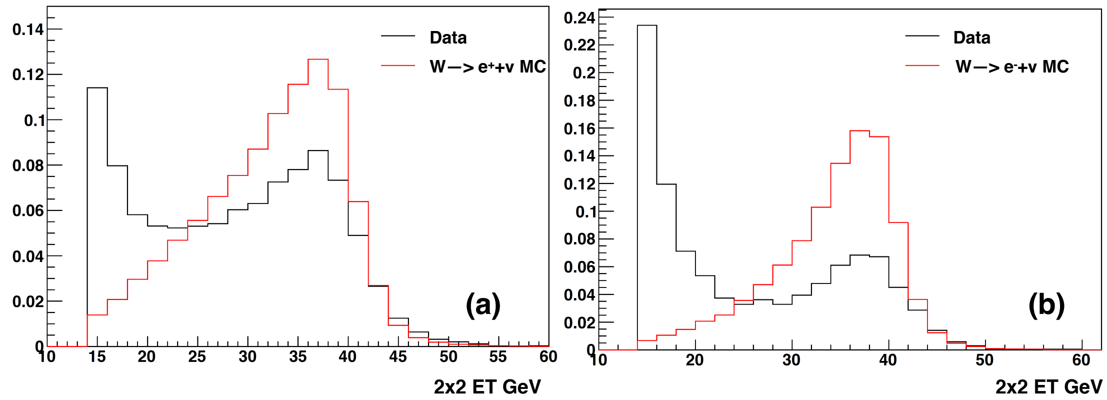

Figure 13: E_T^e distribution of W^+ (a) and W^- (b) candidate events (black) from STAR Run 13 data (after run 13 gains applied), $W \to e\nu$ MC signal (red).

	Run 9 (200 GeV)	**Run 12 (200 GeV)**	**Run 13 (510GeV) period 2**
Run 13 510GeV period 1	$<$ 4 %	$<$ 5%	$>$ 2.5%

Table 2: Comparisons of the absolute gain constants from Run 13 period 1 to Run 13 period 2 and previous years.

5 Systematic Uncertainty

To characterize the uncertainty, the effect of various parameters were examined. After making an estimation on each parameter's effect to E/p, we measured overall systematic uncertainty of the STAR 2013 p-p 510 GeV BEMC calibration to be 3.0 % for period 1 and 2.0 % for period 2.
The most significant contribution was introduced by the dependance on the lower momentum cut. A nominal momentum cut of 2.0 GeV was used as the lower momentum cut in the analysis. The momentum range available in the study was from 1.5 GeV to 10 GeV. Negligible variations in E/p were found for momenta above 10 GeV, while there was significant E/p variation at lower momenta. In the momentum region of 1.5 to 3.5 GeV (1.5 to 3.0 GeV), E/p was found to steady increase for Run 13 period 1 (period 2). The systematic uncertainty due to this momentum dependance was calculated by considering the absolute difference between E/p values at momenta of 1.5 and 3.5 GeV (1.5 and 3.0 GeV) for Run 13 period 1 (period 2). This effect introduced an uncertainty of 2.2% for period 1 and 1.1% for period 2. The momentum dependance of E/p is shown in Figure 14, where E/p shows large variations up to a momentum of about 3 GeV and then becomes stable.

The second most significant contribution to the uncertianty was introduced by the systematic difference between HT and non HT triggered events, as discussed in section 3.1 above. In order to calculate the uncertainty from the trigger bias, three different scenarios each with a different trigger options were considered. The average

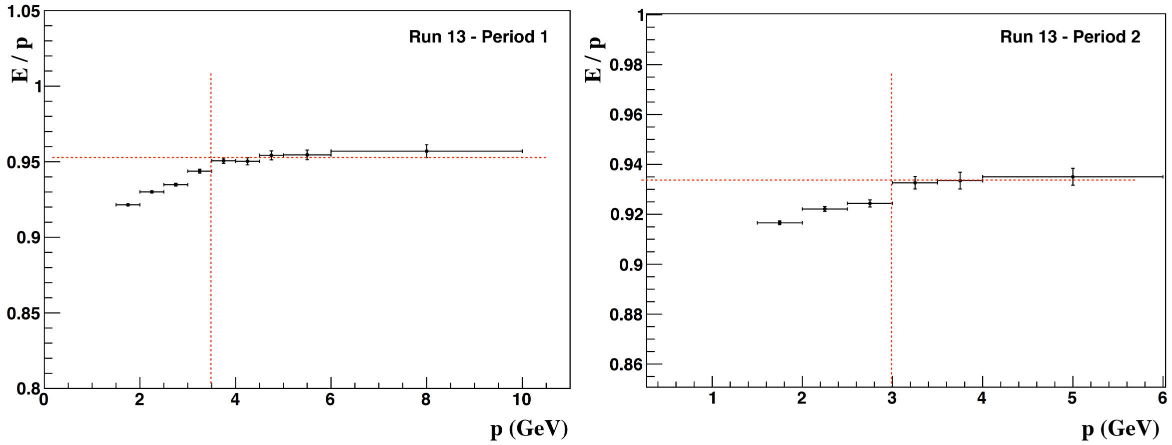

Figure 14: Average E/p as a function of momentum.

E/p value over the whole detector was obtained separately for each scenario. The first scenario (referred to as R_1) used only non HT (JP2) triggered events in the momentum range of 1.5 GeV to 10 GeV. The second scenario (referred to as R_2) used only HT (BHT3) triggered events in the momentum range of 1.5 GeV to 3 GeV. Finally, the third scenario (referred to as $R_{measured}$) used a combination of the two trigger options from scenarios R_1 and R_2 in the momentum ranges specified above. This third trigger option was the trigger option used for the analysis. For the HT trigger, the upper momentum limit was restricted to 3.0 GeV in order to avoid significant bias from the trigger threshold effects. The largest deviation to ($R_{measured}$) from either R_1 or R_2 was then defined as the systematic uncertainty due to the trigger bias. This effect introduced an uncertainty of 1.4 % for Run 13 period 1 and 1.3 % for Run 13 period 2 and is shown in Figure 15.

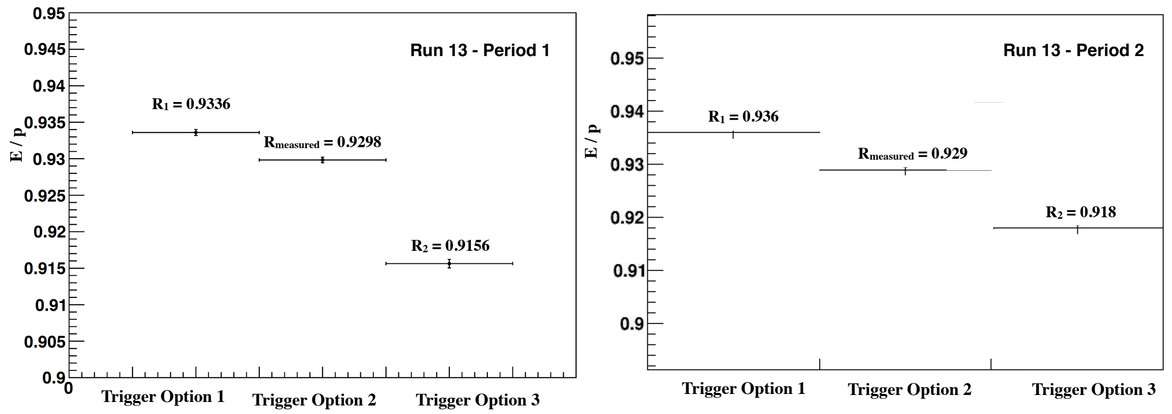

Figure 15: Average E/p for three trigger options.

The dependance of the ΔR cut on E/p was analyzed. In particular, the simulation correction for the tower energy is dependent on the ΔR value. The dependance was checked separately for inner, outer rings and as a whole considering the entire detector. A similar dependance was seen for both the inner and outer rings. Figures 16 and 17 show a small spread of 0.4% (0.3%) of the average E/p around the mean value for the whole detector for period 1(period 2). Therefore no systematic uncertainty due to the

ΔR cut value was assigned for either Run 13 periods 1 or 2.

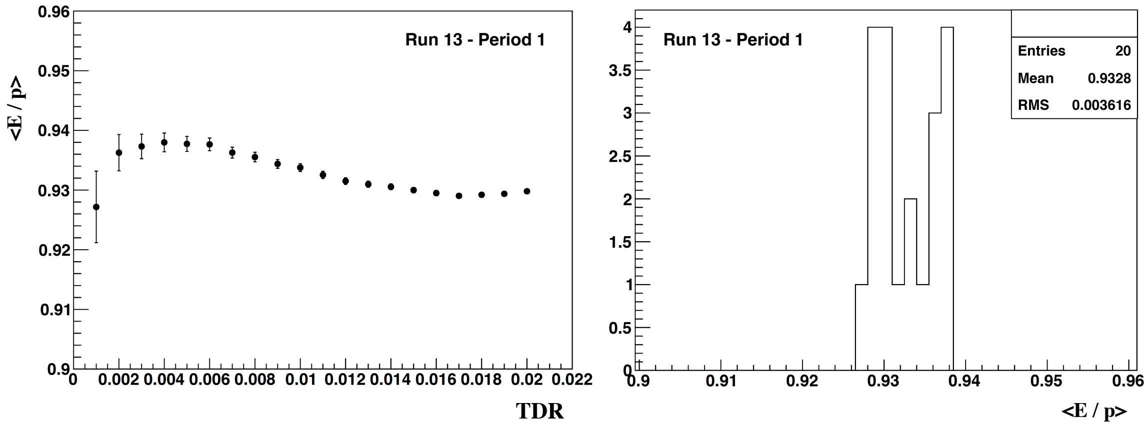

Figure 16: Average E/p as a function of ΔR for period 1.

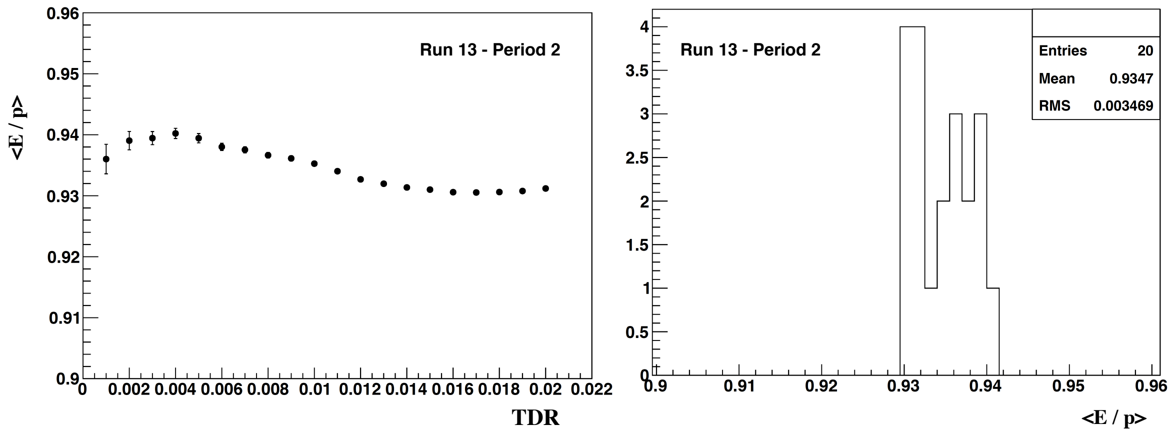

Figure 17: Average E/p as a function of ΔR for period 2.

The time dependance of E/p was estimated by calculating the average E/p for the whole detector per day over the entire Run 13 running period. A systematic dependance of less than 1% was observed for periods 1 and 2. Figures 18 and 19 show the time dependance of the E/p for period 1 (top panels) and period 2 (bottom panels). The left panels plot the average E/p vs. day, while the right panels plot the histograms of the E/p for each of the days. The spread of the E/p around the mean value was assigned as the systematic uncertainty. This effect introduced an uncertainty of 0.8% for period 1 and no uncertainty was assigned for period 2.

The luminosity dependance of E/p was estimated by calculating the average E/p for the whole detector by dividing the data set into several ZDCx ranges. During the period 1 running a small uprising behavior in E/p was noticed with increasing ZDCx rate as shown in Figure 20. The left panel shows the average E/p vs. ZDCx rate, and the right panel shows the E/p spread. The E/p enhancement introduced less than a 0.5 % change at the highest ZDCx rate for period 1. The average E/p for period 2 was found to be even more stable, as shown in Figure 21. Therefore a luminosity dependent systematic uncertainty was not assigned for either periods 1 or 2.

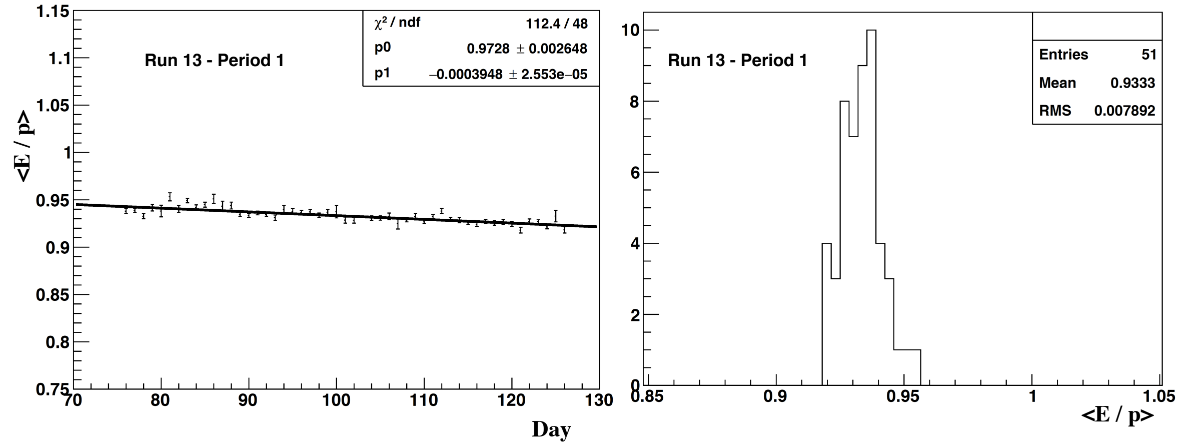

Figure 18: Average E/p for period 1. Left panel: as a function of time (per day), right panel: histogramed E/p values.

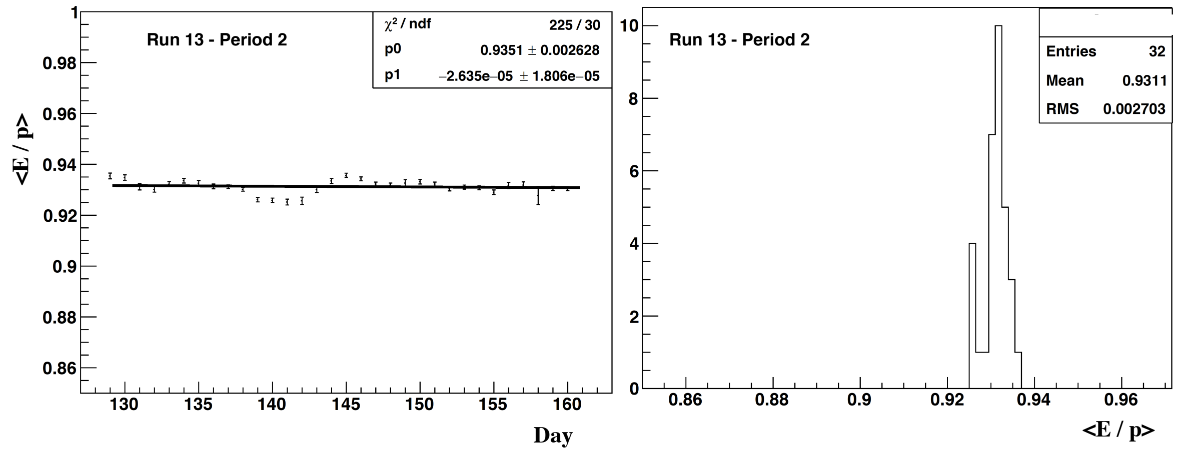

Figure 19: Average E/p for period 2. Left panel: as a function of time (per day), right panel: histogramed E/p values.

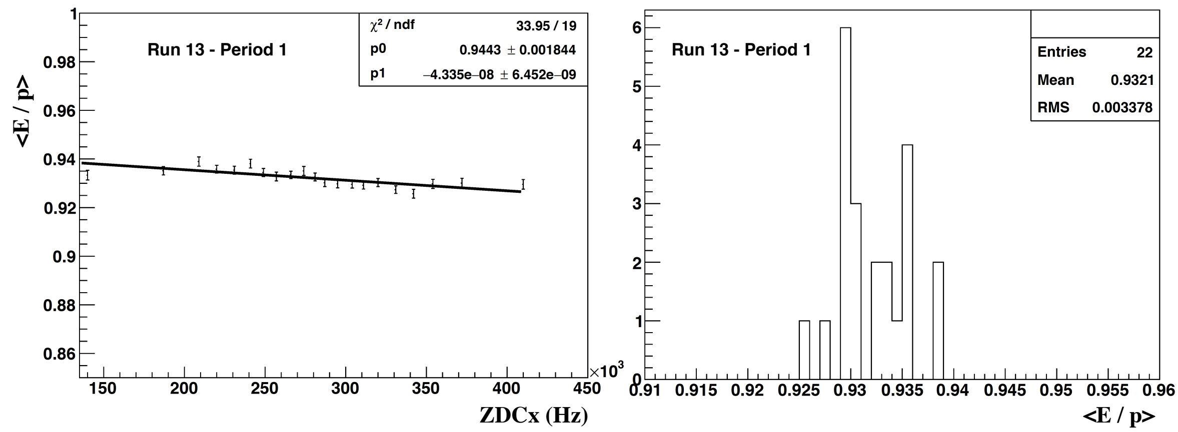

Figure 20: Average E/p for period 1. Left panel: as a function of ZDCx (pb $^{-1}$). Right panel: E/p spread across ZDCx range.

The systematic uncertainty due to the crate dependance was evaluated by calcu-

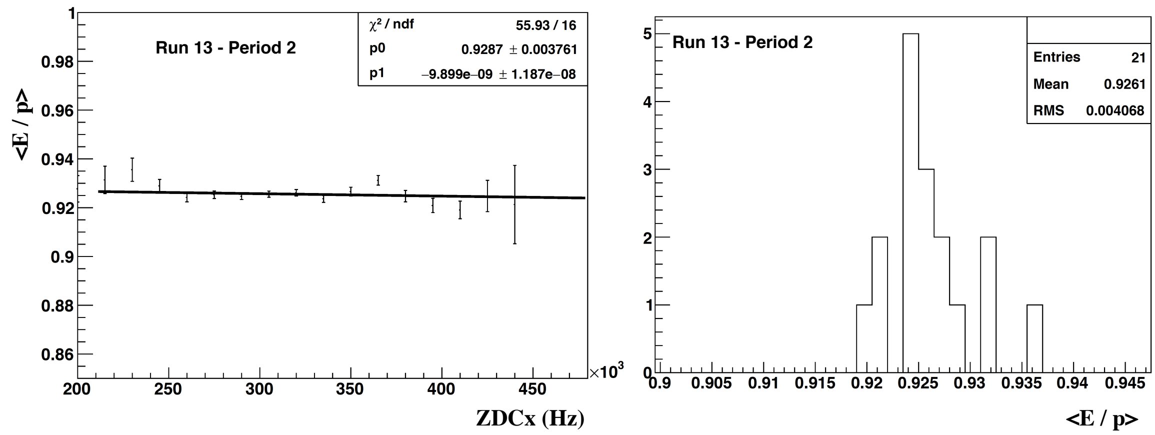

Figure 21: Average E/p for period 2. Left panel: as a function of ZDCx (pb $^{-1}$). Right panel: E/p spread across ZDCx range.

lating the average E/p per crate. Overall, a reasonable spread was observed as shown in Figures 22 and 23 for both period 1 and period 2. The left panels show the average E/p as a function of crate ID, and the right panels show the spread in the E/p values. The spread of E/p between the crates was assigned as the systematic uncertainty. The crate to crate dependance introduced an uncertainty of 1.2% for both period 1 and period 2.

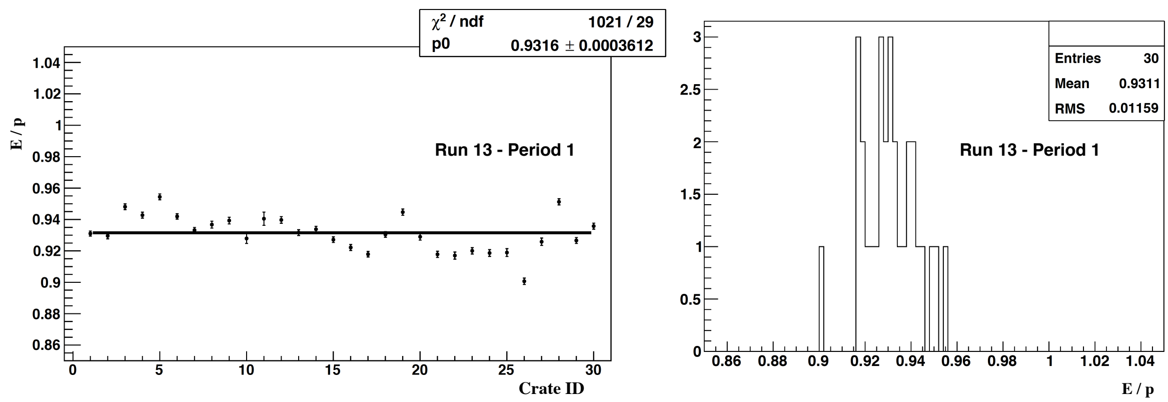

Figure 22: Average E/p per calorimeter crate for period 1. Left panel E/p vs. crate ID. Right panel: Spread of E/p from crate to crate.

The total uncertainty of period 1 comes from adding in quadrature the 1.4% from the trigger bias, 2.2% from the low momentum cut, 0.8% from the time dependance, and 1.2% from the crate dependance, resulting in a 3.0% total systematic uncertainty. Similarly for period 2, total uncertainty of 2.0% is assigned. Table 3 lists the uncertainty contributions and total uncertainty for periods 1 and 2.

6 Conclusion

The BEMC has been successfully calibrated using MIPs and electrons for run 13 pp 510 GeV running period. The calibration uncertainty, quoted as a systematic bias,

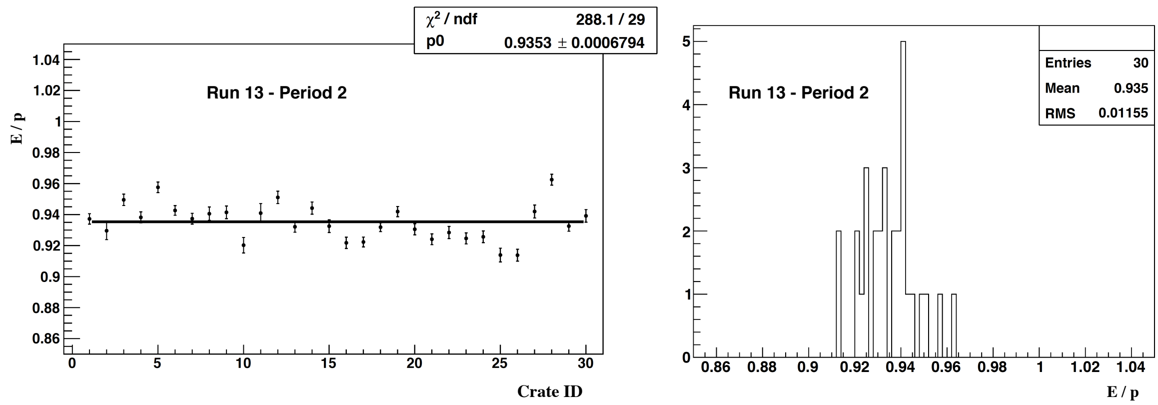

Figure 23: Average E/p per calorimeter crate for period 2. Left panel $E/$ vs. crate ID. Right panel: Spread of E/p from crate to crate.

	Systematic Error Period 1 [%]	**Systematic Error Period 2** [%]
Trigger bias	1.4	1.2
Low momentum cut	2.2	1.1
Tower-track ΔR	0	0
Time Dependance	0.8	0
Luminosity (ZDCx) dependance	0	0
Crate Dependance	1.2	1.2
Total (Added in quatrature)	3.0	2.0

Table 3: Contributions to total systematic uncertainty.

has found to be in the order of run 12 pp 200 GeV calibration. Future calibrations will be able to make use of this study to correct the biases observed here and improve the calibration uncertainty.

Momentum Dependance of HT trigger For HT triggers one expect to have stable E / p for electrons well above the trigger thresholds. But we observed significant momentum dependance well above the trigger thresholds. In particular this was clearly observed for BHT1 trigger. To understand this behavior we have checked various distribution before placing PID cuts which used to remove hadrons tracks from the data sample. After placing dE/dX cut we use nSigmaPion cut to remove remaining hadrons. The cut we used is a linear cut of nSigmaPion equal to 3.0. However when momentum increases such a linear cut of nSigmaPion seems inefficient. The Figure **??** shows distributions of nSigmaPion of BHT1, JP2 and BHT3 triggers. Tower peaks are visible in distributions where electrons are peaks around 4.0. For JP2 and BHT3 trigger two peaks are much separable in comparison to BHT1 trigger. The Figure **??** shows the distributions of nSigmaPion vs E / p in momentum slices of width 1 GeV. Track momentum above 3.5 GeV a clear peak emerge nSigmaPion below 3.0 around E / p equal to 1. These tracks seems to be hadrons measured to have quite a larger energy in the calorimeter towers as a results of the threshold effect. Then the momentum above 6.5 where region well above the thresholds this peak stared to move to the lower E / p values than 1.0. The same behavior can be observe even nSigmaPion above 3.0. Moreover the statistics above 3.0 are very small. Since the cut of nSigmaPion equal to

3.0 is not effective. Therefore when the momentum well above threshold all the tracks in the data sample showing E / p below 1.0 indicating that those are in fact hadrons tracks. In contrast to BHT1 trigger in JP2 trigger **??** one can see a clear peak around E / p around 1.0 in all the momentum regions.

References

[1] https://drupal.star.bnl.gov/STAR/files/userfiles/3475/mid-rapidity-golden-list.csv

[2] https://drupal.star.bnl.gov/STAR/system/files/2009-Calibration-Report.pdf

[3] T.M. Cormier et al., STAR Note 436, 2001 (at http://www.star.bnl.gov)